frontiers in Energy Research

ORIGINAL RESEARCH
published: 20 March 2018
doi: 10.3389/fenrg.2018.00016

# Coin-Cell-Based *In Situ* Characterization Techniques for Li-Ion Batteries

*Liao Zhang[1†], Xiaolong Guo[1†], Jiangtao Huang[1], Yanyu Qu[1], Chaoqun Niu[1], Zhi Du[1], De Li[1,2,3]* and Yong Chen[1,2]**

[1] State Key Laboratory on Marine Resource Utilization in South China Sea, Hainan Provincial Key Laboratory of Research on Utilization of Si-Zr-Ti Resources, College of Materials Science and Chemical Engineering, Hainan University, Haikou, China, [2] Key Laboratory of Advanced Energy Materials Chemistry (Ministry of Education), Nankai University, Tianjin, China, [3] National Laboratory of Solid State Microstructures, Nanjing University, Nanjing, China

*In situ* characterization techniques have made a significant progress in recent years, especially in the electrochemical field. For Li-ion batteries, *in situ* characterization techniques refer to using analytical equipment to directly characterize electrode materials during electrochemical measurements. At present, most *in situ* batteries are developed from commercial simulated batteries, of which the cost is very high and the cycle life is quite short. In this work, two kinds of coin-cell-based *in situ* batteries were designed as *in situ* X-ray diffraction (XRD) and Raman coin cells which exhibit many admirable advantages, such as low cost, long cycle life, easy to carry, and so on. In the designing process, *in situ* XRD and Raman coin cell have been tested with two electrode materials of $Li_4Ti_5O_{12}$ and $LiFePO_4$, and we solved many technical problems of assembling and measuring these two kinds of cells. Finally, *in situ* coin cells could be improved to investigate a variety of electrode materials, and this technique would arouse wide interests in the electrochemical field.

**Keywords: Li-ion battery, coin cell, *in situ* X-ray diffraction, *in situ* Raman, $Li_4Ti_5O_{12}$**

OPEN ACCESS

***Edited by:***
*Da-Wei Wang,*
*University of New South Wales, Australia*

***Reviewed by:***
*Wei Kong Pang,*
*University of Wollongong, Australia*
*Wei Lv,*
*Tsinghua University, China*

****Correspondence:***
*De Li*
*lidenju@sina.com;*
*Yong Chen*
*ychen2002@163.com*

*†These authors have contributed equally to this work.*

***Specialty section:***
*This article was submitted to Energy Storage, a section of the journal Frontiers in Energy Research*

***Received:*** *16 January 2018*
***Accepted:*** *05 March 2018*
***Published:*** *20 March 2018*

***Citation:***
*Zhang L, Guo X, Huang J, Qu Y, Niu C, Du Z, Li D and Chen Y (2018) Coin-Cell-Based In Situ Characterization Techniques for Li-Ion Batteries. Front. Energy Res. 6:16. doi: 10.3389/fenrg.2018.00016*

## INTRODUCTION

Li-ion batteries as a recyclable power source have been used in a variety of electronic devices and energy storage equipment (Armand and Tarascon, 2008), which has aroused a lot of interests in the academic community, while the complicated electrochemical process is still mysterious within Li-ion batteries during the cycling (Qian et al., 2015; Ross, 2015; Wu et al., 2016; Yang et al., 2017). *In situ* characterization techniques are quite suitable to explore the structure-behavior relationship of Li-ion batteries, which can *in situ* observe the electronic structure, the crystal structure, the evolution of micro-morphology, etc. (Yang et al., 2017). In recent years, many *in situ* characterization techniques have been developed, such as *in situ* X-ray diffraction (XRD) (Hu et al., 2014; Liu et al., 2014; Sharma et al., 2015), *in situ* Raman spectroscopy (Gross et al., 2013; Lanz et al., 2013; Wu et al., 2013a), *in situ* Fourier transform infrared spectroscopy (Cheng et al., 2007), and *in situ* transmission electron microscopy (Chen et al., 2015).

Li-ion batteries work in a closed environment to protect the electrode materials from air atmosphere, so it is very difficult to be acquired the internal information of these batteries, except for some *ex situ* characterization techniques after deconstructing the batteries. In order to study the structure change and surface evolution of electrode materials during the electrochemical reactions, many researchers have made great efforts to develop *in situ* techniques for Li-ion batteries. Thurston et al. (1998)

designed an early *in situ* XRD cell to measure electrode materials and intuitively observed lattice expansion and contraction, phase transition, and multi-phase formation. In next two decades, *in situ* XRD cells have been developed sufficiently with a typical construction as follows: a hole was created in a protective case or current collector and next sealed by an X-ray transparent material, such as a Kapton, Be, or Al foil. They were usually based on the simulated battery (Misra et al., 2012; He et al., 2013; Lin et al., 2013, 2014; Roberts et al., 2014; Stancovski and Badilescu, 2014; Villevieille et al., 2014) or the coin cell (Thorne et al., 2011; Fell et al., 2012; Zhu et al., 2013; Lowe and Gao, 2014). The first *in situ* Raman cell was designed by Inaba et al. in 1995, which was used to study the electrochemical Li intercalation into Graphite (Inaba et al., 1995). Shu et al. (2011) also manufactured an *in situ* Raman battery to investigate the electrode material of $Li_4Ti_5O_{12}$. Most *in situ* Raman cells were based on the simulated battery (Long et al., 2011; Nakagawa et al., 2012; Gross et al., 2013; Lanz et al., 2013; Wu et al., 2013b; Hy et al., 2014). However, these *in situ* batteries have not been widely spread in the research community, due to their complicated construction, high cost, and short operation time.

In this work, coin-cell-based *in situ* batteries have been designed and tested for Li-ion batteries. By modifying the normal coin cells, we fabricated *in situ* XRD and Raman coin cells, with which some excellent measurement results are obtained for $Li_4Ti_5O_{12}$ and $LiFePO_4$. Compared with commercial simulated batteries, *in situ* coin cells have many advantages, such as low cost, simple assembly, and good sealing. Thereby, coin-cell-based *in situ* characterization techniques would arouse wide interests in the electrochemical field.

# EXPERIMENT

## Design of *In Situ* Coin Cells

As shown in **Figure 1A**, a normal coin cell was composed of a negative battery case, a battery shrapnel, a lithium anode, a separator, an electrode material, a current collector, and a positive battery case from top to bottom. Based on a normal coin cell, we designed *in situ* XRD and Raman coin cells (**Figures 1B,C**). For *in situ* XRD, a Be sheet as an X-ray windows was firmly attached to the bottom case with a thermoplastic film. Here, the Be sheet was chosen for its high X-ray transmittance and large electrochemical stability window (0–4 V vs. $Li^+/Li$). In the construction, all components were dried in an oven of 80°C for 6 h and then assembled in a glove box filled with Ar gas ($H_2O$, $O_2 < 1$ PPM). Notably, the current collector is a metal mesh with two conductive tails, and the working electrode was toward the X-ray window, instead of the counter electrode in a normal coin cell. The *in situ* Raman coin cell is similar to the *in situ* XRD coin cell, except for an optical window of quartz.

## Preparation of Working Electrode

For *in situ* XRD, one working electrode was prepared as a mixture paste containing 42.5 wt.% $Li_4Ti_5O_{12}$ (Ishihara Sangyo Kaisha, Ltd.), 42.5 wt.% acetylene black, and 15 wt.% polytetrafluoroethylene (PTFE), which was pressed on a stainless steel mesh. Another was prepared as a mixture paste containing 80 wt.% $LiFePO_4$ (Sumitomo Osaka Cement Co. Ltd., Japan), 10 wt.% acetylene black, and 10 wt.% PTFE, which was pressed on an Al mesh (100 mesh) with a mass loading of approximately 5 mg $cm^{-2}$. The counter electrode of lithium metal was separated from the working electrode by a Celgard film 2400 porous polypropylene film, and the electrolyte was 1 M $LiClO_4$ in a mixture of ethylene carbonate (EC)/diethyl carbonate (DEC) (1:1 in volume) or 1 M $LiPF_6$ in a mixture of EC and dimethyl carbonate (DMC) (1:1 in volume).

For *in situ* Raman, the working electrode was composed of 90 wt.% $Li_4Ti_5O_{12}$ and 10 wt.% PTFE which was pressed onto a stainless steel mesh. For comparison, the carbon content was tailored as 10 and 42.5 wt.% in the working electrode. The counter electrode of lithium metal was separated from the working electrode by a Celgard film 2400 porous polypropylene film, and the electrolyte was 1 M $LiClO_4$ in a mixture of EC/DEC (1:1 in volume).

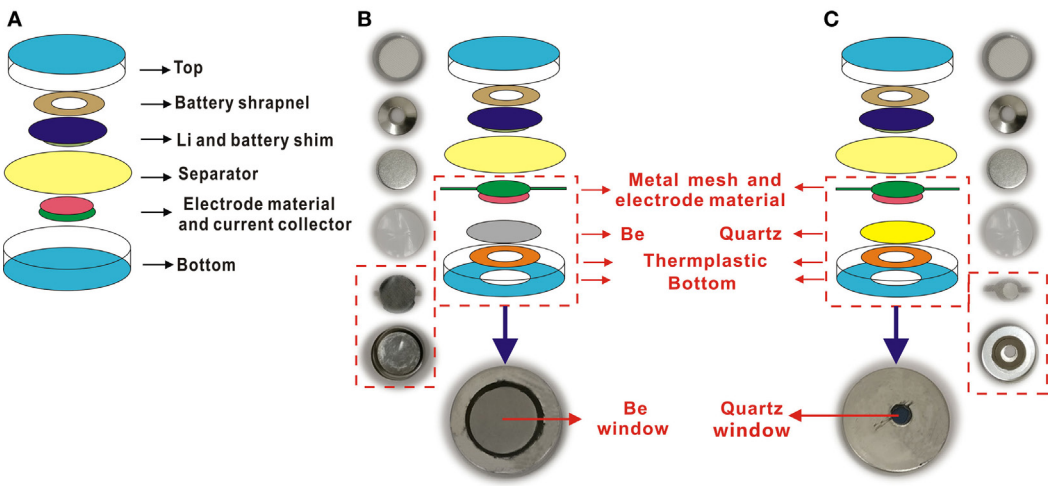


**FIGURE 1** | Structure diagrams and real photos of normal coin cell and *in situ* coin cell. **(A)** Normal coin cell. **(B)** *In situ* X-ray diffraction coin cell. **(C)** *In situ* Raman coin cell.

## *In Situ* Measurements

Electrochemical measurements were conducted on a Battery Testing System (BioLogic VSP-300) at the room temperature, with a potential range of 1.2–2.0 V for $Li_4Ti_5O_{12}$ and 2.8–4.0 V for $LiFePO_4$. Simultaneously, XRD patterns were acquired by using a Bruker D2 PHASER diffractometer with Cu kα radiation, or Raman spectra were collected on Thermo Scientific™ DXR Micro-Raman Spectrometer.

## RESULTS AND DISCUSSION

Our *in situ* XRD/Raman coin cells were tested with the working electrode materials of $Li_4Ti_5O_{12}$ and $LiFePO_4$, and their constructions were optimized according to the experimental results. For *in situ* XRD coin cell, we selected two Be sheets of 0.2 and 0.5 mm thick to *in situ* measure the $LiFePO_4$ electrode. During the charge from 2.8 to 4.0 V with a rate of 0.1 C, *in situ* XRD measurements were conducted simultaneously. As shown in **Figure 2A**, the diffraction peaks of $LiFePO_4$ can be observed for the Be sheet of 0.2 mm thick, but it is difficult for the Be sheet of 0.5 mm thick, as shown in **Figure 2B**, because the thick Be sheet would absorb the X-ray strongly. In the *in situ* XRD pattern of $LiFePO_4$, an XRD peak of $LiFePO_4$ (211) (labeled "T") decreases during the charge process and two XRD peaks of $FePO_4$ (020) and (211) (labeled "H") emerges and increases, which was same as the literature reported in the past (Gibot et al., 2008; Meethong et al., 2012). Thereby, the peak intensity is dependent on the thickness of Be sheet, and the thickness of 0.2 mm is suitable for *in situ* XRD measurements.

It is well known that the sample for XRD measurement must be placed in a fixed plane, and the measured peak would shift with the height of the plane. In our *in situ* XRD coin cell, the thin Be sheet would be bent under a big pressure, which is expected to influence the measured peak more of less. As shown in **Figure 3A**, we prepared two *in situ* XRD coin cells (A-battery and B-battery) with the battery shim of 0.8 and 1.0 mm, respectively. The Be sheet is very flat in A-battery while it is evidently curved in B-battery, owing to the different pressures from the top to the bottom. **Figure 3B** shows XRD patterns of $Li_4Ti_5O_{12}$ measured with these two *in situ* coin cells. The XRD peak of B-battery is obviously broader than that of A-battery, with a quite big peak shoulder in the small angle. Actually, the bent Be sheet made different parts of the working electrode located at different heights, so the broad and asymmetrical peak of B-battery was the superposition of partial XRD peaks at different angles. Thereby, we chose the battery shim of 0.8 mm thick to obtain a flat X-ray window under a proper pressure.

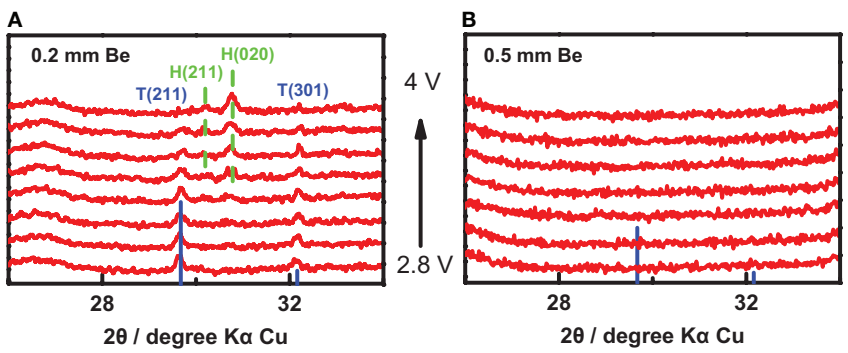


**FIGURE 2** | *In situ* X-ray diffraction (XRD) measurement with different Be sheets. The *in situ* XRD results of $LiFePO_4$ with a Be sheet of **(A)** 0.2 mm and **(B)** 0.5 mm thick, respectively. "H" represents heterosite (lithium-poor phase, $FePO_4$), "T" represents triphylite (lithium-rich phase, $LiFePO_4$).

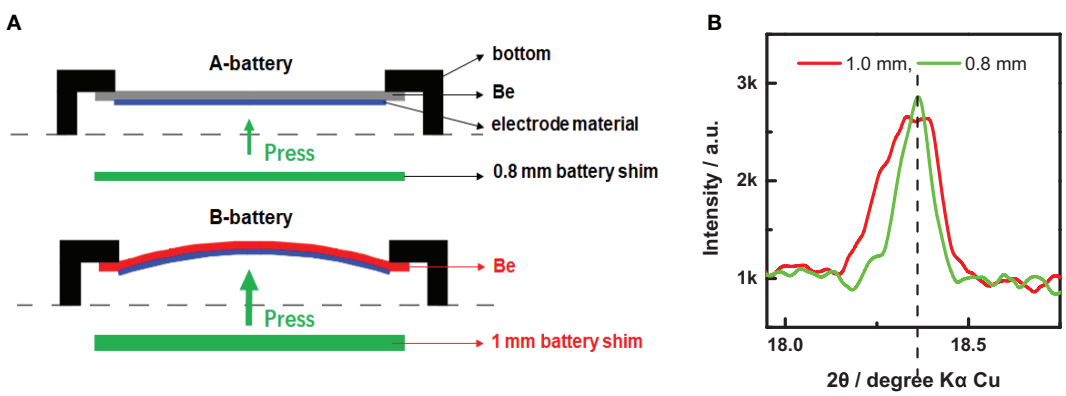


**FIGURE 3** | Influence of the electrode bending on X-ray diffraction (XRD) results. **(A)** Schematics of the flat and bent electrode films pressed on the Be sheets. **(B)** XRD patterns of $Li_4Ti_5O_{12}$ measured with two different *in situ* coin cells in **(A)**.

To check the *in situ* XRD coin cell with different electrolytes, the cathode material of $LiFePO_4$ was measured in a potential range of 2.8–4.0 V with two common electrolytes as 1 M $LiClO_4$ in EC/DEC (1:1 in volume) and 1 M $LiPF_6$ in EC/DMC (1:1 in volume). As shown in **Figure 4**, the charge and discharge curves are quite good for $LiPF_6$, while the charge curve for $LiClO_4$ shows an abnormal plateau at the voltage of 3.8 V. Actually, the abnormal plateau should be attributed to a side reaction, as the $LiClO_4$ with a strong oxidizability might react with the Be sheet at a high voltage. Thus, the electrolyte of $LiPF_6$ (EC/DMC = 1:1 in volume) is proved to be a good choice for the cathode material in the *in situ* XRD coin cell. On the other hand, the anode material of $Li_4Ti_5O_{12}$ can be *in situ* measured excellently for both the electrolytes with a potential range of 1.2–2.0 V.

Using this *in situ* XRD coin cell, we successfully obtained the *in situ* XRD patterns during the electrochemical reaction, as shown in **Figure 5**, which can be deeply analyzed to reveal the structural evolution of electrode materials. For $Li_4Ti_5O_{12}$, the electrochemical measurement was performed as: charge at C/10 to 2.0 V and then potentiostatic within 10 h; discharge at C/10 to 1.2 V and then potentiostatic within 10 h. Simultaneously, *in situ* XRD patterns were acquired every 1 h (including the measurement time of 42 min and the interval time of 18 min). As shown in **Figure 5B**, the red and blue curves were measured during the charge and discharge processes, respectively. The XRD peaks can be excellently fitted with the Lorentzian function to retrieve the peak position, peak intensity, peak area, and full width at half maximum. For Peak (111) of $Li_4Ti_5O_{12}$, the peak position shifted to the small angle during the charge process and then the peak position gradually recovered during the discharge process, as shown in **Figure 5C**. Meanwhile, the peak intensity decreased and recovered during the charge and discharge processes, respectively, as shown in **Figure 5D**. However, the fitting results of peak position and intensity are not so smooth, which should be attributed to the small signal-noise ratio. Furthermore, the peak position and intensity can be used to evaluate the phase fraction and lattice constants, which is significant to study the structural evolution in Li-ion batteries.

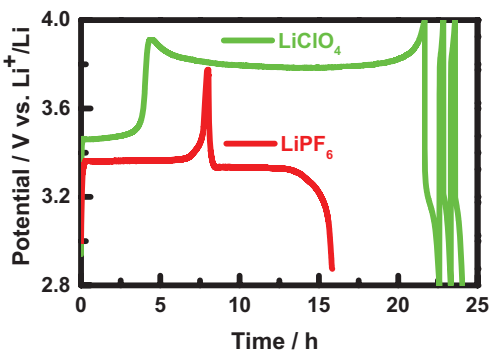


**FIGURE 4** | The charge and discharge curve of *in situ* X-ray diffraction coin cells with different electrolytes as 1 M $LiClO_4$ in a mixture of ethylene carbonate (EC) and diethyl carbonate (1:1 in volume, green) or 1 M $LiPF_6$ in a mixture of EC and dimethyl carbonate (1:1 in volume, red). Here, the charge–discharge measurements were conducted at a current rate of C/10 within a potential range of 2.8–4.0 V.

There also exist some limitations in our design. Although the Be sheet is very popular for *in situ* XRD, Be is very toxic in the form of powder and it can be oxidized easily at a high potential, thus, it was sometimes substituted by Al film or Al-plastic film. In the *in situ* XRD coin cell, the small detective windows limited the mass loading of the working electrode, the edge of coin cell blocked the small-angle diffraction, and the Be sheet absorbed the X-ray especially for the small diffraction angle, which result in a low signal-noise ratio. This problem can be resolved by lengthening the measurement time or enhancing the X-ray intensity. In our lab-based XRD instrument, the low X-ray intensity requires a long collection time to achieve a high signal-noise ratio. In comparison, the synchrotron XRD instrument has a strong X-ray beam with a short wavelength, which can penetrate through *in situ* XRD batteries easily, so the XRD signal is strong enough for the real-time monitoring of electrode materials. However, due to the high intensity, the X-ray of synchrotron might decompose the electrolyte of Li-ion batteries.

On the other hand, the *in situ* Raman coin cell was optimized by tailoring the carbon content in working electrode. We prepared three work electrodes of $Li_4Ti_5O_{12}$ with different carbon contents as 0% C, 5% C, and 42.5% C. As shown in **Figure 6A**, the Raman spectrum of the $Li_4Ti_5O_{12}$ is very close to those previously reported, in which three bands at 238, 433, and 680 $cm^{-1}$ are attributed to O–Li–O bending in the octahedral unit $LiO_6$, Li–O stretching in the tetrahedral unit $LiO_4$, and Ti–O stretching in the octahedral unit $TiO_6$, respectively (Liu et al., 1994; Leonidov et al., 2003; Julien and Zaghib, 2004). Evidently, the signal for 0% C is much stronger than those for 5% C and 42.5% C, and the Raman peaks of PTFE for 0% C were observed as three Raman bands at 1,200–1,400 $cm^{-1}$ region, as shown in **Figure 6B**. However, the conductivity of $Li_4Ti_5O_{12}$ is very poor, and no carbon additive will lead to a large polarization. Contrastively, the Raman D-band and G-band of carbon were observed for 5% C and 42.5% C, and the weak signal should be attributed to the strong optical absorption of carbon.

If the electrode material exhibits a good electrical conductivity, the *in situ* Raman measurement can be directly conducted without the carbon additive. Nevertheless, considering the poor electrical conductivity of some electrode materials, we suggest a potential solution that adopts Surface Enhanced Raman Scattering (SERS), which can be conducted by dropping gold-dielectric nanocomposites on a normal electrode with carbon. Even if the electrode material contains the carbon additive, the Raman signal can be enhanced significantly by the gold-dielectric nanoparticles. To achieve a non-destructive and ultrasensitive SERS, various nanoparticles have been synthesized. Li et al. first reported shell-isolated nanoparticle-enhanced Raman spectroscopy (SHINERS) (Li et al., 2010), and then Yu et al. used the SHINERS to investigate that the by-products and overpotential were reduced in Li–O batteries by water addition (Yu et al., 2017). Similarly, Huang et al. (2013) synthesized a novel Au–Pd bimetallic nanostructure as a platform for highly sensitive monitoring of catalytic reactions by SERS.

Through the quartz window of *in situ* Raman coin cell, the Raman laser is directly illuminated on the working electrode with electrolyte for a long time, so the laser source might influence

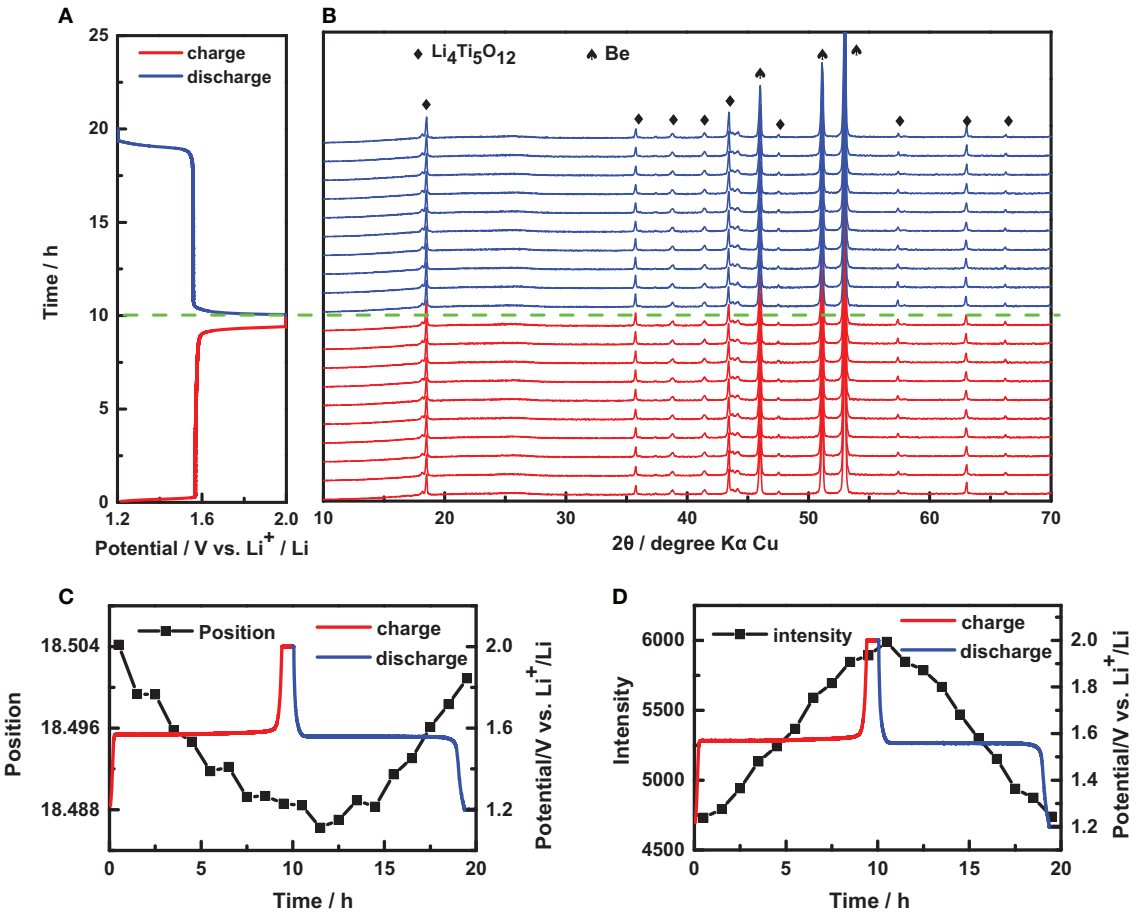


**FIGURE 5** | *In situ* characterization of $Li_4Ti_5O_{12}$ electrode. **(A)** A charge/discharge curve of an *in situ* coin cell with $Li_4Ti_5O_{12}$ electrode: charge at C/10 to 2.0 V and then potentiostatic within 10 h; discharge at C/10 to 1.2 V and then potentiostatic within 10 h. **(B)** *In situ* X-ray diffraction (XRD) patterns of this *in situ* coin cell during the charge and discharge processes. The variation of **(C)** position and **(D)** intensity of peak (111) retrieved from *in situ* XRD patterns in **(B)**.

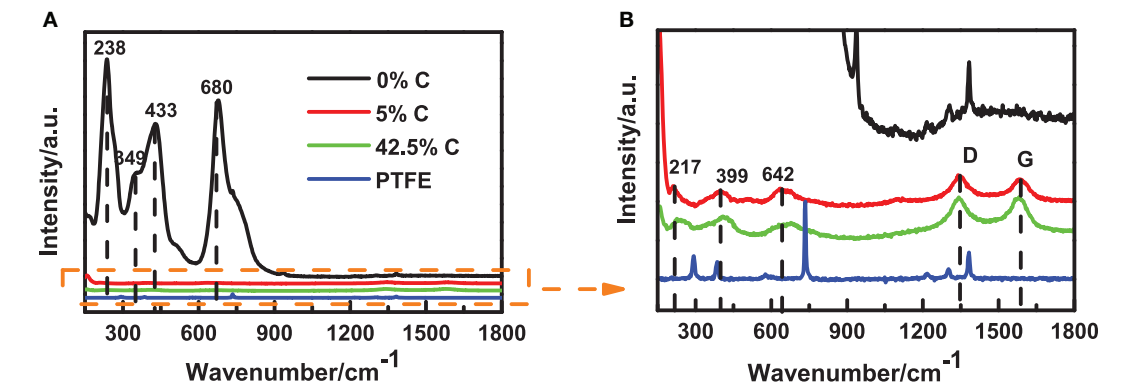


**FIGURE 6** | Raman spectra of $Li_4Ti_5O_{12}$ electrodes with different carbon contents. **(A)** Raman spectra of three $Li_4Ti_5O_{12}$ electrodes and **(B)** enlarged view of **(A)**.

the measurement. Thus, two identical *in situ* Raman coin cells are assembled with the working electrode of $Li_4Ti_5O_{12}$ and the electrolyte of 1 M $LiClO_4$ in EC/DEC (1:1 in volume), and we adopted two different Raman laser sources for comparison. As a result, the Raman spectrum of $Li_4Ti_5O_{12}$ was very stable for the wavelength of 780 nm, while the Raman D-band and G-band of carbon emerged after 10 min for the wavelength of 532 nm, as shown in **Figure 7**. By further increasing the measuring time,

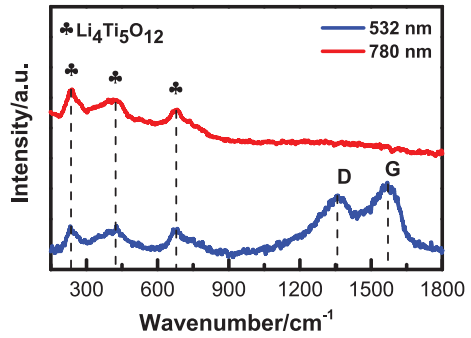


**FIGURE 7** | Raman spectra of $Li_4Ti_5O_{12}$ electrodes measured by using different laser sources, with the laser wavelength of 532 and 780 nm for the blue and red curves, respectively.

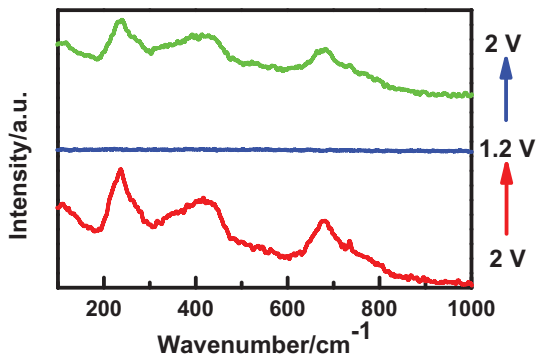


**FIGURE 8** | *In situ* Raman spectra of $Li_4Ti_5O_{12}$ electrode. The Raman spectrum evolved as the charged electrode (bottom red curve) was discharged to 1.2 V (middle blue curve) and then charged to 2.0 V (top green curve).

only carbon signal can be observed in the spectrum for the wavelength of 532 nm. Obviously, the electrolyte was decomposed and carbonized seriously under the illumination of short-wavelength laser. Thereby, *in situ* measurement can be conducted for a long time by using the long-wavelength laser with a low photon energy.

By using our *in situ* Raman coin cell, the *in situ* Raman spectra were collected for the working electrode of $Li_4Ti_5O_{12}$, as shown in **Figure 8**. At the charged state, we observed the typical Raman bands of $Li_4Ti_5O_{12}$. After discharge, these Raman bands disappeared clearly, while they recovered after recharge. These phenomena are excellently consistent with early literatures (Schneider et al., 2011; Shu et al., 2011). Currently, it is still not clear about the disappearance of Raman signal in this case. Normally, it might be owing to structure change during phase transition (Schneider et al., 2011). In addition, $Li_4Ti_5O_{12}$ material becomes electrically conductive after discharge, and then the optical skin depth of the laser will be reduced, which in turn will lead to the disappearance of Raman signals. Therefore, the *in situ* Raman signals can be used to study the local structures and variations, which is quite useful to reveal the structure degradation in Li-ion batteries.

However, *in situ* Raman was rarely adopted in Li-ion batteries for some problems. In the *in situ* Raman coin cell, the conductive agent of carbon would seriously suppress the Raman signals in the working electrode, which can be overcome by using the SERS technique as dropping gold-dielectric nanocomposites on a normal electrode with carbon. To prevent the decomposition of electrolyte, we can replace the short-wavelength laser with the long-wavelength laser, while some vibrational modes might be lost in the new Raman spectrum. During continuous charging and discharging, the fluorescent background would be increased with the electrolyte decomposition, resulting in a weak Raman signal considerably.

## CONCLUSION

In this work, we designed the *in situ* XRD/Raman coin cells and optimized their configurations by testing the working electrodes of $Li_4Ti_5O_{12}$ and $LiFePO_4$. In the *in situ* XRD coin cell, the Be sheet of 0.2 mm thick was chosen to reduce the X-ray absorption, and the internal pressure was tailored to prevent bending the thin Be sheet. The electrolyte of $LiPF_6$ was proved to be a good choice for both cathode and anode materials, while the electrolyte of $LiClO_4$ could not be adopted for the cathode materials. From the *in situ* XRD results, the peak position and intensity can be used to evaluate the phase fraction and lattice constants, which is significant to study the structural evolution in Li-ion batteries. On the other hand, in the *in situ* Raman coin cell, the conductive agent of carbon would suppress the Raman signals in the working electrode, which can be resolved by reducing the carbon content for conductive electrode materials or adopting SERS for normal electrodes. The long-wavelength laser was better for in *situ* Raman measurements, for the electrolyte of Li-ion batteries would be decomposed and carbonized seriously under the illumination of short-wavelength laser. According to the *in situ* Raman results, the local structures and variations can be investigated to reveal the structure degradation in Li-ion batteries. Therefore, *in situ* coin cells could be improved to investigate a variety of electrode materials, and this technique would arouse wide interests in the electrochemical field.

## AUTHOR CONTRIBUTIONS

YC directed the project, DL took charge of this investigation, LZ optimized *in situ* cells, analyzed the data, and authored the manuscript, XG designed the original *in situ* cells, and all authors contributed to the discussion.

## FUNDING

This work was financially supported by the NSFC (No. 21603048 and No. 51362009), Natural Science Foundation of Hainan (Grant No. 20165186), the Science and Technology Development Special Fund Project (ZY2016HN07), the International Science & Technology Cooperation Program of Hainan (KJHZ2015-02), and the Hainan University's Scientific Research Foundation (kyqd1545).

## REFERENCES


Armand, M., and Tarascon, J. M. (2008). Building better batteries. *Nature* 451, 652–657. doi:10.1038/451652a

Chen, X., Li, C., and Cao, H. (2015). Recent developments of the in situ wet cell technology for transmission electron microscopies. *Nanoscale* 7, 4811–4819. doi:10.1039/c4nr07209j

Cheng, Y., Wang, G., Yan, M., and Jiang, Z. (2007). In situ analysis of interfacial reactions between negative MCMB, lithium electrodes, and gel polymer electrolyte. *J. Sol. St. Electrochem.* 11, 310–316. doi:10.1007/s10008-006-0122-2

Fell, C. R., Chi, M., Meng, Y. S., and Jones, J. L. (2012). In situ X-ray diffraction study of the lithium excess layered oxide compound $Li[Li_{0.2}Ni_{0.2}Mn_{0.6}]O_2$ during electrochemical cycling ☆. *Solid State Ionics.* 207, 44–49. doi:10.1016/j.ssi.2011.11.018

Gibot, P., Casascabanas, M., Laffont, L., Levasseur, S., Carlach, P., Hamelet, S., et al. (2008). Room-temperature single-phase Li insertion/extraction in nanoscale $Li_xFePO_4$. *Nat. Mater.* 7, 741–747. doi:10.1038/nmat2245

Gross, T., Giebeler, L., and Hess, C. (2013). Novel in situ cell for Raman diagnostics of lithium-ion batteries. *Rev. Sci. Instrum.* 84, 1278–1319. doi:10.1063/1.4813263

He, H., Huang, C., Luo, C. W., Liu, J. J., and Chao, Z. S. (2013). Dynamic study of Li intercalation into graphite by in situ high energy synchrotron XRD. *Electrochim. Acta* 92, 148–152. doi:10.1016/j.electacta.2012.12.135

Hu, C. W., Chen, T. Y., Shih, K. S., Wu, P. J., Su, H. C., Chiang, C. Y., et al. (2014). Real-time investigation on the influences of vanadium additives to the structural and chemical state evolutions of $LiFePO_4$ for enhancing the electrochemical performance of lithium-ion battery. *J. Power Sources* 270, 449–456. doi:10.1016/j.jpowsour.2014.07.138

Huang, J., Zhu, Y., Lin, M., Wang, Q., Zhao, L., Yang, Y., et al. (2013). Site-specific growth of Au-Pd alloy horns on Au nanorods: a platform for highly sensitive monitoring of catalytic reactions by surface enhancement Raman spectroscopy. *J. Am. Chem. Soc.* 135, 8552–8651. doi:10.1021/ja4004602

Hy, S., Felix, F., Chen, Y. H., Liu, J. Y., Rick, J., and Hwang, B. J. (2014). In situ surface enhanced Raman spectroscopic studies of solid electrolyte interphase formation in lithium ion battery electrodes. *J. Power Sources* 256, 324–328. doi:10.1016/j.jpowsour.2014.01.092

Inaba, M., Yoshida, H., Ogumi, Z., Abe, T., Mizutani, Y., and Asano, M. (1995). ChemInform abstract: in situ Raman study on electrochemical Li intercalation into graphite. *Cheminform* 26, 20–26. doi:10.1149/1.2043869

Julien, C. M., and Zaghib, K. (2004). Electrochemistry and local structure of nanosized $Li_{4/3}Me_{5/3}O_4$ (Me = Mn, Ti) spinels. *Electrochimica Acta* 50, 411–416. doi:10.1016/j.electacta.2004.03.052

Lanz, P., Villevieille, C., and Novák, P. (2013). Electrochemical activation of $Li_2MnO_3$ at elevated temperature investigated by in situ Raman microscopy. *Electrochim. Acta.* 109, 426–432. doi:10.1016/j.electacta.2013.07.130

Leonidov, I. A., Leonidova, O. N., Perelyaeva, L. A., Samigullina, R. F., Kovyazina, S. A., and Patrakeev, M. V. (2003). Structure, ionic conduction, and phase transformations in lithium titanate $Li_4Ti_5O_{12}$. *Phys. Solid State* 45, 2183–2188. doi:10.1134/1.1626760

Li, J. F., Huang, Y. F., Ding, Y., Yang, Z. L., Li, S. B., Zhou, X. S., et al. (2010). Shell-isolated nanoparticle-enhanced Raman spectroscopy. *Sci. Found. China* 464, 392–395. doi:10.1038/nature08907

Lin, C. K., Ren, Y., Amine, K., Qin, Y., and Chen, Z. (2013). In situ high-energy X-ray diffraction to study overcharge abuse of 18650-size lithium-ion battery. *J. Power Sources* 230, 32–37. doi:10.1016/j.jpowsour.2012.12.032

Lin, X., Ma, R., Shao, L., Shui, M., Wu, K., Wang, D., et al. (2014). In-situ X-ray diffraction study on the structural evolutions of oxidized fluorophosphates as anode materials for lithium-ion batteries. *Ceram. Int.* 40, 9107–9120. doi:10.1016/j.ceramint.2014.01.125

Liu, D. Z., Hayes, W., Kurmoo, M., Dalton, M., and Chen, C. (1994). Raman scattering of the $Li_{1+x}Ti_{2-x}O_4$ superconducting system. *Phys. C Supercond.* 235, 1203–1204. doi:10.1016/0921-4534(94)91826-0

Liu, Q., He, H., Li, Z. F., Liu, Y., Ren, Y., Lu, W., et al. (2014). Rate-dependent, Li-ion insertion/deinsertion behavior of $LiFePO_4$ cathodes in commercial 18650 $LiFePO_4$ cells. *ACS Appl. Mater. Interfaces* 6, 3282. doi:10.1021/am405150c

Long, B. R., Chan, M. K. Y., Greeley, J. P., and Gewirth, A. A. (2011). Dopant modulated Li insertion in Si for battery anodes: theory and experiment. *J. Phys. Chem. C* 115, 18916–18921. doi:10.1021/jp2060602

Lowe, M. A., and Gao, J. (2014). Mechanistic insights into operational lithium-sulfur batteries by in situ X-ray diffraction and absorption spectroscopy. *RSC Adv.* 4, 18347–18353. doi:10.1039/c4ra01388c

Meethong, N., Kao, Y. H., Tang, M., Huang, H. Y., Carter, W. C., and Chiang, Y. M. (2012). Electrochemically induced phase transformation in nanoscale olivines $Li_{1-x}MPO_4$ (M = Fe, Mn). *Chem. Mater.* 20, 6189–6198. doi:10.1021/cm801722f

Misra, S., Liu, N., Nelson, J., Hong, S. S., Yi, C., and Toney, M. F. (2012). In situ X-ray diffraction studies of (De)lithiation mechanism in silicon nanowire anodes. *ACS Nano* 6, 5465. doi:10.1021/nn301339g

Nakagawa, H., Domi, Y., Doi, T., Ochida, M., Tsubouchi, S., Yamanaka, T., et al. (2012). In situ Raman study on degradation of edge plane graphite negative-electrodes and effects of film-forming additives. *J. Power Sources* 206, 320–324. doi:10.1016/j.jpowsour.2012.01.141

Qian, D., Ma, C., More, K. L., Meng, Y. S., and Chi, M. (2015). Advanced analytical electron microscopy for lithium-ion batteries. *NPG Asia Mater.* 7, e193. doi:10.1038/am.2015.50

Roberts, M. R., Madsen, A., Nicklin, C., Rawle, J., Palmer, M. G., Owen, J. R., et al. (2014). Direct observation of active material concentration gradients and crystallinity breakdown in $LiFePO_4$ electrodes during charge/discharge cycling of lithium batteries. *J. Phys. Chem. C Nanomater. Interfaces* 118, 6548–6557. doi:10.1021/jp411152s

Ross, F. M. (2015). Opportunities and challenges in liquid cell electron microscopy. *Science* 350, aaa9886. doi:10.1126/science.aaa9886

Schneider, H., Maire, P., and Novák, P. (2011). Electrochemical and spectroscopic characterization of lithium titanate spinel $Li_4Ti_5O_{12}$. *Electrochim. Acta* 56, 9324–9328. doi:10.1016/j.electacta.2011.08.008

Sharma, N., Tapiaruiz, N., Singh, G., Armstrong, A. R., Pramudita, J. C., Brand, H. E. A., et al. (2015). Rate dependent performance related to crystal structure evolution of $Na_{0.67}Mn_{0.8}Mg_{0.2}O_2$ in a sodium-ion battery. *Chem. Mater.* 27, 150928134805001. doi:10.1021/acs.chemmater.5b02142

Shu, J., Shui, M., Xu, D., Gao, S., Yi, T., Wang, D. J., et al. (2011). Design and comparison of ex situ and in situ devices for Raman characterization of lithium titanate anode material. *Ionics* 17, 503–509. doi:10.1007/s11581-011-0544-4

Stancovski, V., and Badilescu, S. (2014). ChemInform abstract: in situ Raman spectroscopic-electrochemical studies of lithium-ion battery materials: a historical overview. *J. Appl. Electrochem.* 44, 23–43. doi:10.1007/s10800-013-0628-0

Thorne, J. S., Dahn, J. R., Obrovac, M. N., and Dunlap, R. A. (2011). An in situ study of the electrochemical reaction of Li with amorphous/nanostructured Cu6Sn5 + C. *J. Electrochem. Soc.* 158, A1328. doi:10.1149/2.040112jes

Thurston, T. R., Jisrawi, N. M., Mukerjee, S., Yang, X. Q., Mcbreen, J., Daroux, M. L., et al. (1998). Synchrotron x-ray diffraction studies of the structural properties of electrode materials in operating battery cells. *Appl. Phys. Lett.* 69, 194–196. doi:10.1063/1.117369

Villevieille, C., Sasaki, T., and Novák, P. (2014). Novel electrochemical cell designed for operando techniques and impedance studies. *RSC Adv.* 4, 6782–6789. doi:10.1039/c3ra46184j

Wu, J., Dathar, G. K., Sun, C., Theivanayagam, M. G., Applestone, D., Dylla, A. G., et al. (2013a). In situ Raman spectroscopy of $LiFePO_4$: size and morphology dependence during charge and self-discharge. *Nanotechnology* 24, 424009. doi:10.1088/0957-4484/24/42/424009

Wu, J., Leng, G., Xu, X., Li, K., Lao, X., and Zhou, C. (2013b). In-situ synthesis of a cordierite-andalusite composite for solar thermal storage. *Sol. Energy Mater. Sol. Cells* 108, 9–16. doi:10.1016/j.solmat.2012.08.010

Wu, J., Shan, H., Chen, W., Gu, X., Tao, P., Song, C., et al. (2016). In situ environmental TEM in imaging gas and liquid phase chemical reactions for materials research. *Adv. Mater. Weinheim* 28, 9686–9712. doi:10.1002/adma.201602519

Yang, Y., Liu, X., Dai, Z., Yuan, F., Bando, Y., Golberg, D., et al. (2017). In situ electrochemistry of rechargeable battery materials: status report and perspectives. *Adv. Mater.* 29, 1606922. doi:10.1002/adma.201606922

Yu, Q., Wu, S., Jin, Y., Yang, S., Guo, S., Yang, S., et al. (2017). From O2− to HO2−: reducing by-products and overpotential in Li-$O_2$ batteries by water addition. *Angew. Chem. Int. Ed. Engl.* 56, 4960–4964. doi:10.1002/anie.201611122

Zhu, W., Liu, D., Trottier, J., Gagnon, C., Mauger, A., Julien, C. M., et al. (2013). In-situ X-ray diffraction study of the phase evolution in undoped and Cr-doped

$Li_xMn_{1.5}Ni_{0.5}O_4$ (0.1≤ x ≤1.0) 5-V cathode materials. *J. Power Sources* 242, 236–243. doi:10.1016/j.jpowsour.2013.05.021

**Conflict of Interest Statement:** The authors declare that the research was conducted in the absence of any commercial or financial relationships that could be construed as a potential conflict of interest.